Ion debris characterization from a *z*-pinch extreme ultraviolet light source

Erik L. Antonsen,[a] Keith C. Thompson, Matthew R. Hendricks, Darren A. Alman, Brian E. Jurczyk, and D. N. Ruzic
Plasma-Materials Interaction Group, University of Illinois at Urbana-Champaign, Urbana, Illinois 61801

(Received 24 June 2005; accepted 23 January 2006; published online 21 March 2006)

An XTREME Technologies XTS 13-35 extreme ultraviolet (EUV) light source creates a xenon *z* pinch that generates 13.5 nm light. Due to the near x-ray nature of light at this wavelength, extremely smooth metal mirrors for photon collection must be employed. These are exposed to the source debris. Dissolution of the *z*-pinch gas column results in high-energy ion and neutral release throughout the chamber that can have adverse effects on mirror surfaces. The XTREME commercial EUV emission diagnostic chamber was designed to maximize diagnostic access to the light and particulate emissions from the *z* pinch. The principal investigation is characterization of the debris field and the erosive effects on optics present. Light emission from the *z* pinch is followed by ejection of multiply charged ions and fast neutral particles that make up an erosive flux to chamber surfaces. Attenuation of this erosive flux to optical surfaces is attempted by inclusion of a debris mitigation tool consisting of foil traps and neutral buffer gas flow. Characterization of the *z*-pinch ejecta is performed with a spherical sector energy analyzer (ESA) that diagnoses fast ion species by energy-to-charge ratio using ion time-of-flight (ITOF) analysis. This is used to evaluate the debris tool's ability to divert direct fast ions from impact on optic surfaces. The ITOF-ESA is used to characterize both the energy and angular distribution of the direct fast ions. Xe^{+} up to Xe^{+4} ions have been characterized along with Ar^{+} (the buffer gas used), W^{+}, Mo^{+}, Si^{+}, Fe^{+}, and Ni^{+}. Energy spectra for these species from 0.5 up to 13 keV are defined at 20° and 30° from the pinch centerline in the chamber. Results show a drop in ion flux with angular increase. The dominant species is Xe^{+} which peaks around 8 keV. Ion flux measured against buffer gas flow rate suggests that the direct fast ion population is significantly attenuated through increases in buffer gas flow rate. This does not address momentum transfer from scattered ions or fast neutral particles. These results are discussed in the context of other investigations on the effects of total particle flux to normal incidence mirror samples exposed for 1×10^7 pulses. The samples (Si/Mo multilayer with Ru capping layer, Au, C, Mo, Pd, Ru, and Si) were exposed to the source plasma with 75% argon flow rate in the debris mitigation tool and surface metrology was performed using x-ray photoelectron spectroscopy, atomic force microscopy, x-ray reflectivity, and scanning electron microscopy to analyze erosion effects on mirrors. These results are compared to the measured direct ion debris field. © *2006 American Institute of Physics*. [DOI: 10.1063/1.2175471]

I. INTRODUCTION

Extreme ultraviolet (EUV) lithography is currently a leading candidate for the manufacture of integrated circuits at the 32 nm node and below. Before this technology can be put into high-volume use, however, several critical issues need to be solved. One challenging problem in moving EUV lithography from the drawing board to the manufacturing floor is operation of a satisfactory light source in conjunction with collector optics required for light capture. There are currently two prospects for EUV light sources being considered. The first is a laser-produced plasma[1,2] (LPP) which uses a pulsed laser to ablate a solid fuel source and create high temperatures required for EUV light generation. The second option is a discharge-produced plasma[1] (DPP) which uses a gaseous *z* pinch to compress plasmas to high temperatures, generating the ion species required for EUV light emission. Both of these source options generate a significant amount of debris, such as energetic ions, that necessarily interacts with collector optics in the source chamber causing erosion and deposition of materials on the mirrors. Ultimately these debris mechanisms degrade mirror reflectivity, decoupling the light source from the rest of the manufacturing process. The current study focuses on fast ion generation from the DPP source using xenon as the emissive material. Characterization of the fast ion debris is critical to creating an operational junction between light source and collector optics because of mirror erosion that occurs due to heavy ion impact. Low-energy sputtered debris can also cause reflectivity degradation through deposition and coating processes, but these effects appear to be minimal compared to erosive fluxes encountered in the source chamber. This appears to be due to the presence of the debris mitigation tool.

Generation of debris is an inherent problem in the DPP source since the postemission time frame requires expansion of the *z*-pinch gases away from the pinch location, along with nominal electrode material erosion and acceleration. The XTREME Technologies XTS 13-35 EUV light source is a DPP source currently used to provide light for lithography in the MS-13 EUV Micro Exposure Tool (MET) produced by

[a]Electronic mail: eantonse@uiuc.edu

0021-8979/2006/99(6)/063301/8/$23.00 © 2006 American Institute of Physics

Downloaded 30 Nov 2007 to 130.126.32.13. Redistribution subject to AIP license or copyright; see http://jap.aip.org/jap/copyright.jsp

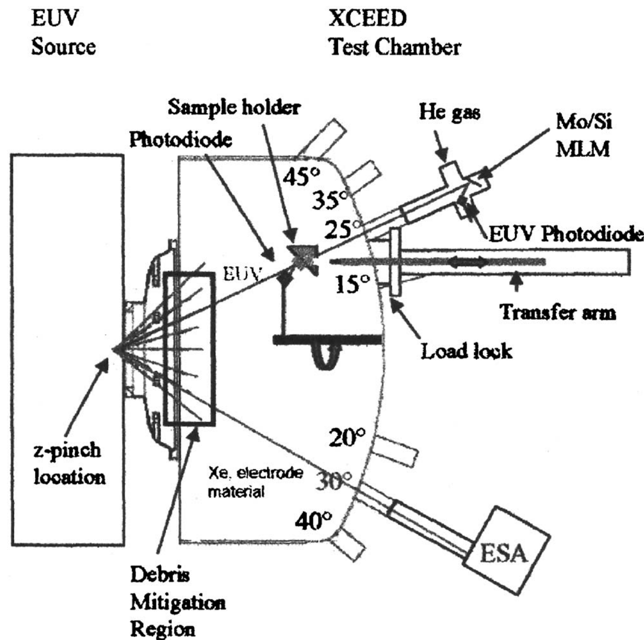

FIG. 1. The XCEED test chamber allows diagnostic access at 5° increments from 15° to 45° off the z-pinch axis.

Exitech Ltd. This same source is under investigation at the University of Illinois at Urbana-Champaign to investigate the generation and expansion of the debris produced, its effect on exposed optics, and possible new mitigation schemes. To address this problem, a debris mitigation tool was designed by XTREME Technologies[3] and applied to the source. It consists of multiple foil traps[4] and a neutral gas curtain. Ideally this type of mitigation is directed at scattering of fast ions by the gas curtain such that the expanding ion front is redirected into the foil trap and extinguished. This allows photon passage through the debris tool while minimizing ion passage to the collector optics.

This paper is directed toward characterizing the fast ion debris in terms of species and energy spectra using a spherical sector energy analyzer. The direct fast ion debris field is characterized with the debris tool operating at varying buffer gas flow rates. Additionally, angular variations in ion species and energy spectra are investigated. Section II describes the experimental apparatus used. In Sec. III, experimental results of the ion debris analysis are presented for species, energy spectra, buffer gas flow rate dependence, and angular distribution. In Sec. IV these data are compared with results from microanalysis of mirror surfaces exposed to the source for long time frames are discussed. Also, EUV light intensity is discussed focusing on absorption from the ambient chamber pressure. Conclusions are drawn in Sec. V.

II. APPARATUS AND APPROACH

The XTREME commercial EUV emission diagnostic (XCEED) experimental test chamber is a custom design built to mate to the XTS 13-35 source[3] for diagnostic access. A schematic of the chamber with spherical sector energy analyzer (ESA) access is shown in Fig. 1. The source flows xenon gas into a small chamber where preionization occurs, initiating a 15 J discharge resulting in a z-pinch plasma column. The self-compression of this column results in heating sufficient to generate Xe^{8+} to Xe^{12+} ions capable of emitting EUV light at 13.5 nm. Photons must pass through the debris mitigation tool before exiting the source for collection. A debris mitigation tool is provided by XTREME Technologies GmbH. The location of the mitigation region is shown in Fig. 1 at the junction between the test chamber and adapter. Mirror sample exposures are run for up to 4×10^7 pulses. During these tests, samples placed in the chamber are removed periodically using a load-lock system.

EUV source emission is monitored using International Radiation Detectors, Inc. (IRD) Ti/Zr/Si 6/480/50 nm photodiodes capable of measuring 13.5 nm. This photodiode is positioned at the 35° port. It is used in a single reflection system from a 40 bilayer Mo/Si mirror with a 4 nm Si capping layer. The reflectivity is ~70%. The mirror is housed behind a 1 mm orifice and backfilled with He gas. This is intended to minimize ion damage to the mirror.

The ESA (Refs. 5–7) is a well-characterized diagnostic capable of measuring ion energy and discriminating by charge state. These experiments use a Comstock[8] model AC-902B™ with dual microchannel plate (MCP) detectors from Burle Corporation (model CP-618C™).[9,10] The analyzer has line-of-sight access to the source through 2–3/4 in. conflat. (CF) ports positioned at angular intervals of 5° from 15° to 45° from the centerline of the pinch. Access at 0° is impeded by the beam stop of the debris tool. Current experiments are performed at 20° and 30° angles. Data acquisition for the ESA is triggered by the rising light signal from the photodiode. The ESA is mounted on a bellows connection to the chamber for three-dimensional pointing control. A 1 mm orifice located proximal to the ESA limits flow to the diagnostic. The entrance orifice to the ESA deflector section is 3 mm in diameter and total distance traversed by the ions from the source to the microchannel plates is 150 cm. Targeting to the z pinch is performed by leveling the ESA with respect to the chamber, and adjusting the horizontal angle of the connection bellows such that the ESA sweeps across the exit vector of the source ions. At 256 Hz operation, the ESA signal is maximized. A laser from the ESA entrance location is aimed at a target on the flange connection to the tank. Location is marked and the ESA is stabilized at signal maximum. This also allows evaluation of scattered ions by targeting slightly off the z-pinch emission vector into the chamber. The layout for the diagnostic is shown in Fig. 2. Ions that successfully traverse the distance from the plasma source to the entrance orifice of the ESA are discriminated against based on energy-to-charge ratio. The spherical sectors of the energy analyzer are charged to equal voltages of opposite sign. The inner sector is negatively charged and the outer is positively charged for proper ion deflection. This creates an electric field inside the device, which turns ions through the 160° of curvature where they impact microchannel plate detectors. Ions that are too fast are not turned sufficiently and extinguish against the outer sector wall. Similarly, ions of insufficient velocity are overdeflected and extinguish against the inner sector wall. The governing equation is

Downloaded 30 Nov 2007 to 130.126.32.13. Redistribution subject to AIP license or copyright; see http://jap.aip.org/jap/copyright.jsp

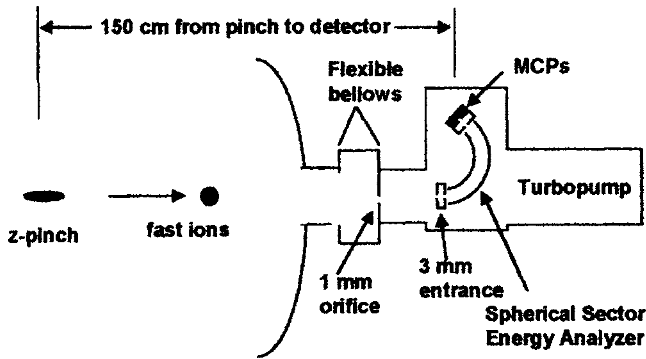

FIG. 2. The ESA is mounted on a flexible bellows with a 1 mm orifice limiting flow and allowing differential pumping.

$$\frac{E}{q} = -\frac{\Delta V}{(r_1/r_2 - r_2/r_1)}, \tag{1}$$

where E is the ion energy (eV), q is the ionization charge state, ΔV is the voltage difference between the spherical sectors, r_1 and r_2 are the radii of the inner (4.88 cm) and outer (6.02 cm) sectors, respectively. The resolution of the energy analyzer is described by

$$\frac{\Delta E}{E} = \frac{\omega}{[R(1-\cos\varphi) + \delta \sin\varphi]}, \tag{2}$$

where R is the mean sphere radius ($\sim$5.47 cm), ω is the aperture size, φ is the included angle of the analyzer (160°), and δ is the distance from the exit of the sector field to the final exit aperture (1.07 cm). The entrance aperture used is 3 mm, however, the effective aperture size is actually smaller since access to the ESA is limited by a 1 mm orifice used for differential pumping. Using this aperture size, the resolution for an 8 keV ion is ±72.8 eV.

To make the conversion from "hits" measured on the histogram function of the oscilloscope to actual ions reaching the detector, an experimental calibration is performed. The setup consists of firing a SPECS (Ref. 11) model IQE 11/35™ ion gun with xenon gas feed at a 1 mm orifice. Figure 3 shows a schematic of this setup. The xenon is ionized to Xe^+ and accelerated to 1 keV nominally. Behind the orifice is placed a Comstock model FC610™ Faraday cup to collect the current. The current measured in this setup is 0.33 nA. The Faraday cup and ESA location are swapped and the ESA then measures the same ion flow from the gun. Since the ESA only measures a small fraction of the total ions emitted, several data points are taken to characterize the ion energy spectra emitted from the gun. Current measured by the Faraday cup takes into account all ions from the gun striking the cup surface. However, the ESA at 974 keV measures ±9 eV according to Eq. (2). Therefore, the actual ESA signal is created by a fraction of the total ions measured by the Faraday cup. This fraction is the ratio of the area under the peak value with uncertainty divided by the total area under the energy spectra of the ion gun and is calculated to be 0.143. This is shown in Fig. 4. The width of the ESA measurements around the peak value is 18 eV. This reflects a bin size ($2\Delta E$) that can be used to produce a histogram as shown in Fig. 4. The area covered by this histogram allows calculation of the number of ions per hit. For the calibration, ΔE does not change significantly from 875–1100 eV. Similarly, when calculating total ion flux from the source, ΔE is calculated from Eq. (2) and is dependent on the ion energies measured by the ESA at given voltages.

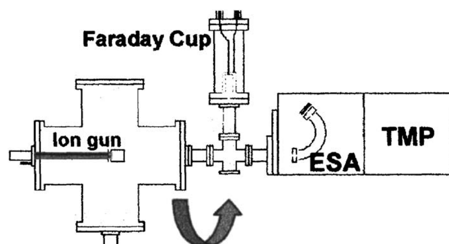

FIG. 3. Schematic for the experimental calibration of the ESA. The ion gun is locked in place and the Faraday cup and ESA exchange positions in front of the gun (TMP=turbomolecular pump).

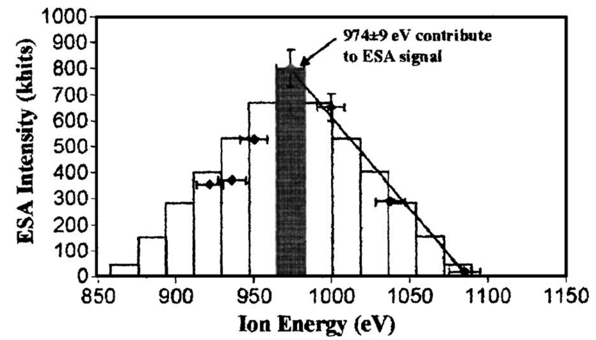

FIG. 4. 14.3% of ions measured by the Faraday cup contribute to the peak ESA measurement.

The number of ions measured is given by

$$N_i(E) = \frac{X(E)(I/e)t\,\%\,\Delta E}{X(1\text{ keV})DE(E)/DE(1\text{ keV})}, \tag{3}$$

where $N_i(E)$ is the number of ions at a given energy E, $X(E)$ is the measured number of hits at a given energy E, I is the current measured from the Faraday cup (0.33 nA), e is the elementary charge (1.6×10^{-19} C), t is the measurement time (1.656 s), $\%\Delta E$ is the percentage of contributing ions shown in Fig. 5 (0.143), X (1 keV) is the number of ESA hits measured at the ion gun peak energy (803 khits), and the DE ratio is the detector efficiency at the given energy, divided by

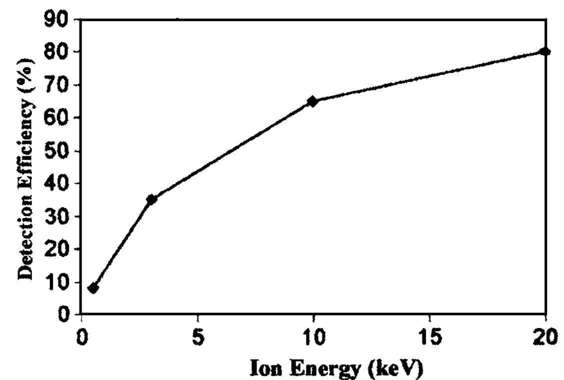

FIG. 5. Detection efficiency for positive ion impact on the microchannel plate detectors (see Ref. 9).

Downloaded 30 Nov 2007 to 130.126.32.13. Redistribution subject to AIP license or copyright; see http://jap.aip.org/jap/copyright.jsp

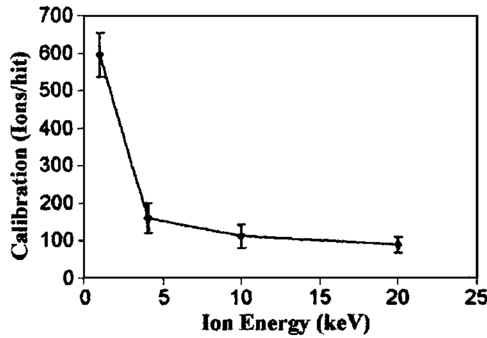

FIG. 6. ESA calibration as a function of ion energy for positive ion impact.

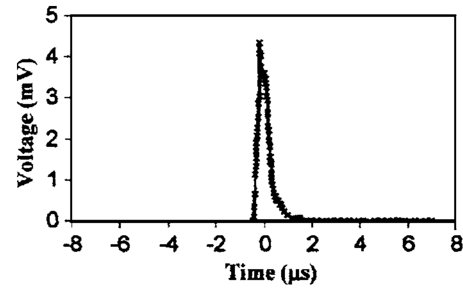

FIG. 7. Typical signal from the control photodiode used to trigger the ESA.

the detector efficiency at 1 keV. We assume here that secondary electrons are absorbed by the Faraday cup such that each single ion impacting the cup transfers a single charge. Figure 5 shows detection efficiencies for the energy range of interest. This data is taken from Burle Corporation[10] concerning secondary electron emission from positive ions impacting MCPs.

At 1 keV the detection efficiency is 10%. An 8 keV ion measured during pinch testing has a detection efficiency of 55%. Figure 6 shows the calibration curve as a function of ion energy. This is $N_i(E)/X(E)$ from Eq. (3). The equation for ion flux is then

$$\Gamma(E) = \frac{N_i(E)}{2AN\Delta E}, \tag{4}$$

where $N_i(E)$ is the number of ions at a given energy E, A is the area of the entrance orifice (0.007 58 cm^2), N is the total number of pulses (61 440), and ΔE is given by Eq. (2). The factor of two is due to defining the bin size as $\pm\Delta E$. Total uncertainty is calculated using the equation for the calibration and known uncertainties. Uncertainty in the orifice area is neglected here as well as in the total number of pulses taken. The uncertainty in the peak number of hits is 69 khits or 8.2%. Uncertainty for the ΔE term is a function of the voltages on the deflector plates that are known to be within ±20 V. For an 8 keV ion, the plate voltage is about 1600 V. Using two plates, this translates to an uncertainty of 2.5%. Finally, the uncertainty on the detector efficiencies is about 3%, so taking into account the ratio used, the total uncertainty there is about 4.2%. Compiling these values, an uncertainty of 9.7% of the ion flux is obtained for ion calibration.

III. EXPERIMENTAL RESULTS

The source is operated at a pulse rate of 256 Hz. The oscilloscope is triggered on the rise of the EUV signal from the photodiode. The typical photodiode signal is shown in Fig. 7. For the ESA ion measurements, the histogram function on the oscilloscope allows additive counting of pulses over a set time frame. There is significant electromagnetic interference when insulated gate bipolar transistor (IGBT) switches in the source circuit fire, and it is not possible to completely remove the noise signal from this. However, at $t=10\ \mu$s postdischarge, the IGBT noise ends and all data after that point are recorded. Figure 8 shows a picture of the histogram along with labels for the peaks shown. Each data set is taken over 4 min of integration time while the histogram function counts the pulses in each time bin. This particular trace is taken at an E/q value of 2.667 keV/charge and an argon flow rate of 10% of the maximum flow.

Peak identification is performed by comparing relative time frame and abundances with expected signals from elements known to be present in the chamber. The Xe^+ and Xe^{2+} ion signatures are distinct, and given the known travel distance (150 cm), the arrival time matches predicted values for given E/q ratios. Inserting known mass and expected charge states of other elements allows characterization of the other peaks recorded. Each of the peaks corresponds to an element found in the pinch vicinity or on the path of ions to the pinch. Tungsten, molybdenum, silicon, iron, and nickel are found in various sources in the chamber. The largest peaks correspond to the first two ionization states of xenon.

By varying the flow rate of the buffer gas in the chamber, the effects on ion fluxes are measured. This allows quantification of fast ion interruption on the path to the collector optics. Figures 9–12 show the drop in ion flux for all species measured as the argon flow rate increases at an angle of 20° from the pinch centerline. The exception in the $E/q=2$ keV case is the Ar^+. Possible reasons for the measured increase are discussed below. For the cases of $E/q=4$, 8, and 13 keV, ion species magnitude consistently drops with an increase in the buffer gas flow rate. This is seen across all species measured.

At 30° from the pinch centerline, ion fluxes are measured again. Figures 13–16 show ion flux by species for increasing argon flow rates. As with the 20° case, most species show a decrease in ion flux as argon flow rate increases. However, Xe^+ shows an increase from 0% to 10% of the

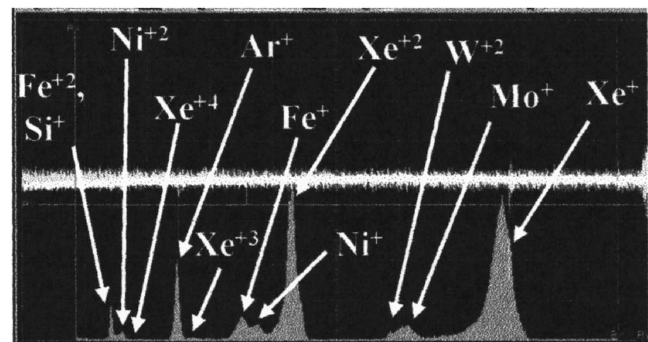

FIG. 8. Oscilloscope image of the ion species peaks discriminated by the ESA-ITOF. The histogram was integrated for 4 min at 256 Hz.

Downloaded 30 Nov 2007 to 130.126.32.13. Redistribution subject to AIP license or copyright; see http://jap.aip.org/jap/copyright.jsp

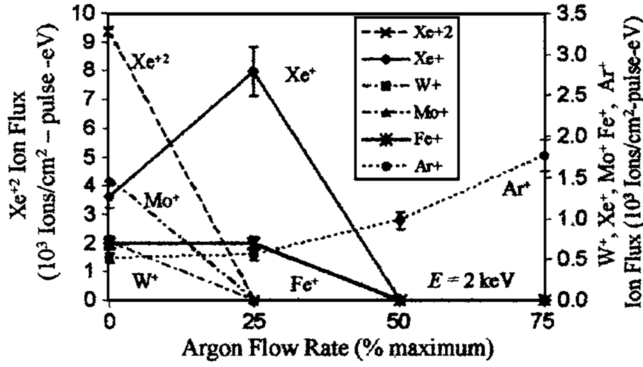

FIG. 9. Ion fluxes for E=2 keV at 20° from centerline.

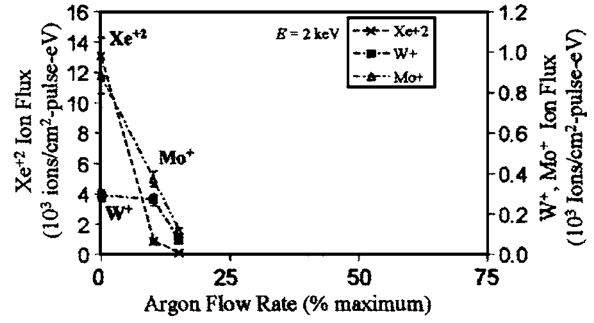

FIG. 13. Ion fluxes for E=2 keV at 30° from centerline.

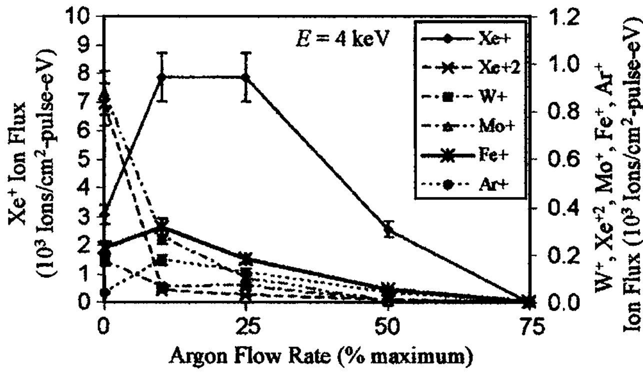

FIG. 10. Ion fluxes for E=4 keV at 20° from centerline.

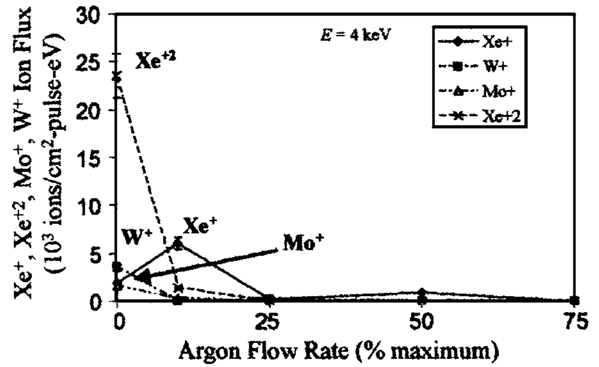

FIG. 14. Ion fluxes for E=4 keV at 30° from centerline.

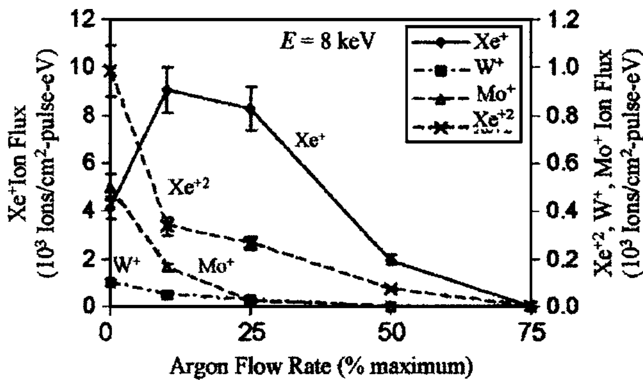

FIG. 11. Ion fluxes for E=8 keV at 20° from centerline.

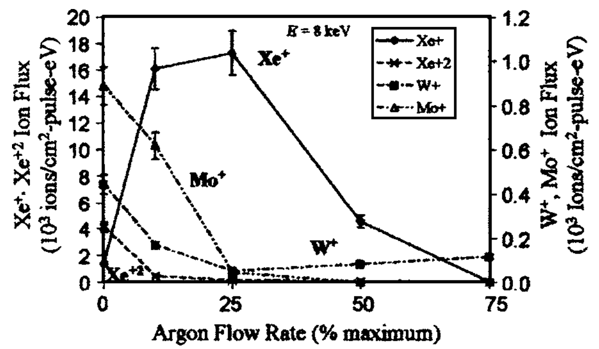

FIG. 15. Ion fluxes for E=8 keV at 30° from centerline.

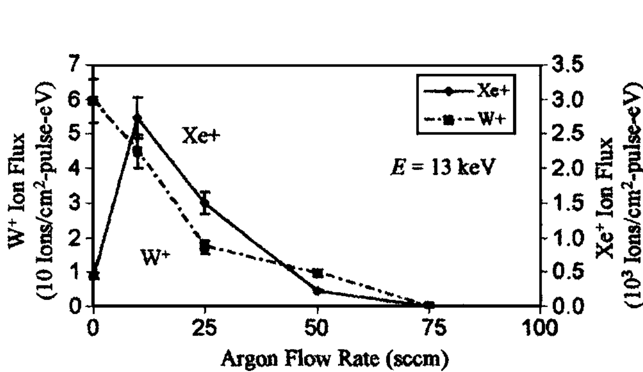

FIG. 12. Ion fluxes for E=13 keV at 20° from centerline.

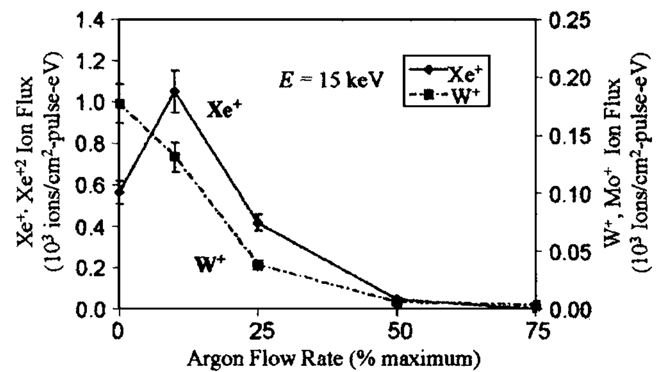

FIG. 16. Ion fluxes for E=15 keV at 30° from centerline.

Downloaded 30 Nov 2007 to 130.126.32.13. Redistribution subject to AIP license or copyright; see http://jap.aip.org/jap/copyright.jsp

maximum buffer gas flow rate for all energies. Additionally, at 8 keV it continues to increase until 25% argon flow. Reasons for this are discussed in Sec. IV.

The ion abundance for each species measured is considered as a function of ion energy for buffer gas flow rates varying from 0% to 50% of the maximum flow rate. Figures 17–20 show this data at 20° from the pinch centerline. Xe^{+} ions generally maximize at about 8 keV and dominate the measured data at all flow rates. Xe^{+2} is also seen consistently at all flow rates. Xe^{+3} and Xe^{+4} are both measured in Fig. 18 with small but relevant peaks. High-energy multiply ionized species are not well measured because interference from current switching from large IGBT switches in the source interfere with any measurement before 10 μs.

For the case of 30° from the pinch centerline, ion energy spectra are again characterized for given argon flow rates in Figs. 21–23. For no argon flow, species seem to maximize around 1 keV and level out at higher energies. At higher flow rates, Xe^{+}, W^{+}, and Mo^{+} maximize around 8 keV. The change in ion hit intensity from 20° to 30° is shown in Fig. 24. There is an apparent drop in all species with the exception of Fe^{+} and possibly W^{+}.

IV. DISCUSSION

Data above show depletion of high-energy ion species measured as the buffer gas curtain pressure is increased. This could be due to two possible mechanisms. If simple charge exchange from high-energy Xe with buffer gas is occurring, then a particle of lower charge but equal momentum will pass the debris tool with the possibility of impacting mirror surfaces. However, if ejected particles are being scattered through interactions with the buffer gas curtain, then deflection into the foil trap is likely and the damaging particle momentum is expected to be attenuated. For a comprehensive assessment of the utility of the debris tool, measurements of neutral particle passage through the tool must be taken. Additionally, scattered ion effects must be accounted for. Both these measurements are being investigated for future work.

For 20° and 30° cases, as buffer gas flow rates are increased, most ion species show a decline in ion flux consistent with increased scattering levels. The exception to this trend is Xe^{+}, which shows an increase in ion flux up to 10% maximum buffer gas flow (25% maximum buffer gas flow for the case of 8 keV ions). Possible reasons for this include optimization of pinch conditions with the additional density and ion mobility provided by the smaller argon ions. The most likely explanation is the conversion of Xe^{+2} to Xe^{+} by charge exchange. Note that at zero flow rate, Xe^{+2} is the dominant species. However, it is important to note that around 75% of the maximum argon flow rate, all ion species fail to be detected by the ESA. This indicates that the debris tool is successful in mitigating direct fast ion impact at the location of the entrance aperture of the ESA (96 cm). This correlates with past data from XTREME that shows that the debris tool results in significant increase in mirror reflectivity lifetime.[1] This data makes no statements concerning scattered ion or fast neutral contributions to erosion.

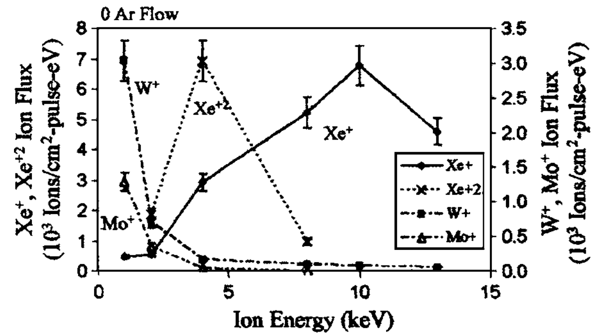

FIG. 17. Ion energy spectra for no argon flow at 20° from centerline.

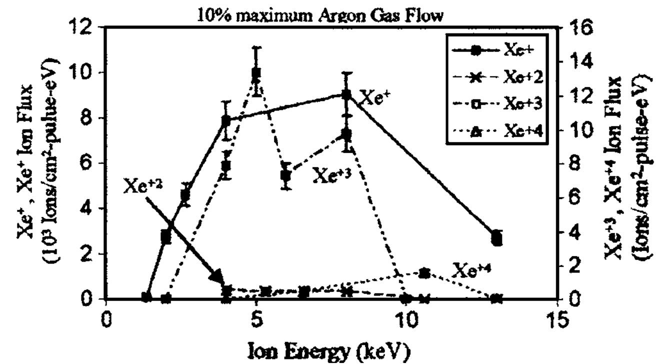

FIG. 18. Ion energy spectra for 10% maximum argon flow at 20° from centerline.

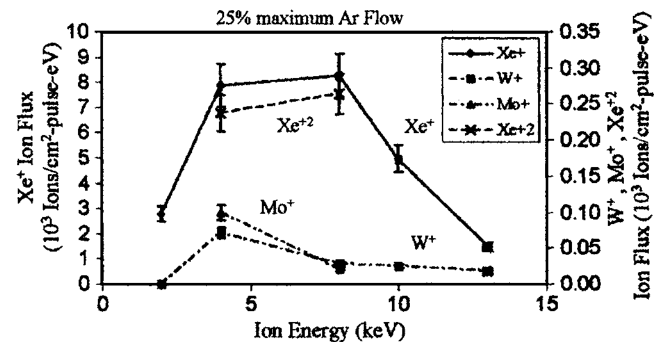

FIG. 19. Ion energy spectra for 25% maximum argon flow at 20° from centerline.

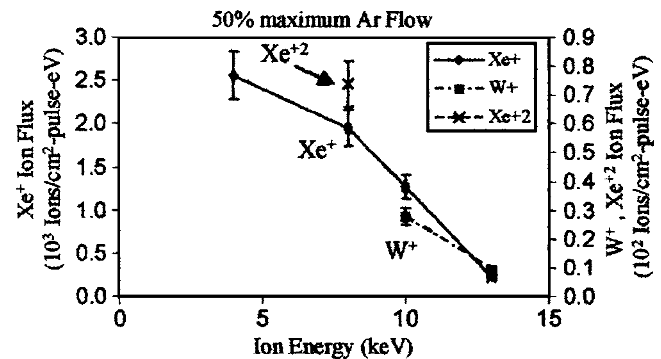

FIG. 20. Ion energy spectra for 75% maximum argon flow at 20° from centerline.

Downloaded 30 Nov 2007 to 130.126.32.13. Redistribution subject to AIP license or copyright; see http://jap.aip.org/jap/copyright.jsp

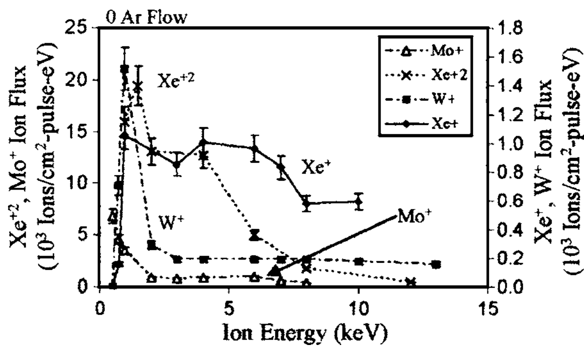

FIG. 21. Ion energy spectra for no argon flow at 30° from centerline.

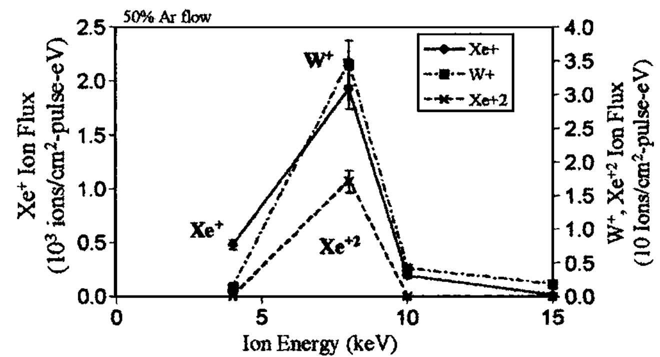

FIG. 23. Ion energy spectra for 50% maximum argon flow at 30° from centerline.

Figures 17–20 show measured ion energy spectra for the 20° case. Xe^+ dominates the ion flux for most argon flow rates. Xe^{+2} shows significant presence when no argon is flowing through the debris tool, but is markedly lower than Xe^+ levels when argon is flowing. This suggests that once neutral gas is present, significant charge exchange collisions occur to reduce the measurement of higher charge states. Figures 21–23 show measured ion spectra for the 30° case. There is a similar trend to the 20° case for no argon flow. However, Xe^{+2} levels are increased significantly at 30° compared to 20°. At 25% and 50% maximum buffer gas flow, ion flux magnitudes across species are lower than the cases for 20°.

The largest contribution to ion ejection is by far Xe^+. This species maximizes at 8 keV in the presence of buffer gas. Xe^{+2} also contributes, maximizing at 8 keV with buffer gas. Most of the ion species decrease in intensity with an angular increase from 20°–30°. These include Xe^+, Xe^{+2}, Fe^+, and Mo^+. W^+ appears to maintain about the same or slightly greater ion flux level between the two angles. A decrease in ion flux with angle suggests that pinch instabilities direct the bulk of the escaping ion flow in the axial direction. This is expected with xenon ion species, which originate within the z-pinch column. However, metal ions from the sources in the vicinity of the pinch are not necessarily directed by kink instability.

A 4×10^7 pulse exposure test[12] was performed with mirror samples removed at 1×10^7 pulses for microscopic analysis. Microscopic analyses are presented in Refs. 12 and 13 and are summarized here for comparison with fast ion debris data from ESA analyses. The pulse frequency was 64 Hz and argon flow in the debris mitigation tool was 75% of maximum. Samples were exposed at normal incidence (mirror surface at 80° to the incident light) and included a Mo/Si bilayer with Ru capping layer, Au, C, Mo, Pd, Ru, and Si. X-ray photoelectron spectroscopy (XPS) analysis from mirror samples show W^+ embedded in the Mo sample that could only have come from the electrode materials. This indicates that some heavy ions are transported through the debris tool even though the ESA may not be measuring such a low level. Additionally, data from atomic force microscopy (AFM) and x-ray reflectivity (XRR) showed an increase in surface roughness between two to six times after the 1×10^7 shot exposure. Scanning electron microscopy (SEM) data shows erosion of 10 nm for Mo, 13 nm for Mo/Si, and 54 nm for Au. The implication from this data is that erosive flux from the source is not completely stopped by the debris tool at the 75% maximum argon flow rate. However, an assessment of acceptable levels of debris can only be performed through reflectivity measurements, since this is the ultimate metric for system operability. Reflectivity measurements with the debris tool indicate that debris tool operation significantly increases mirror lifetime.[1] This suggests that the mechanism of debris tool operation is likely significant ion scattering by the buffer gas into the foil trap with a small percentage of charge exchange that does not relieve total particle momentum transfer to mirrors. It is also likely, as discussed above, that with a significant decrease in direct fast ion impact, there are still residual levels of scattered ion and fast neutral erosive flux that is unaccounted for in these experiments.

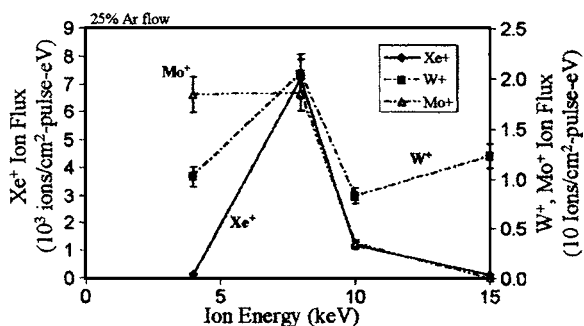

FIG. 22. Ion energy spectra for 10% maximum argon flow at 30° from centerline.

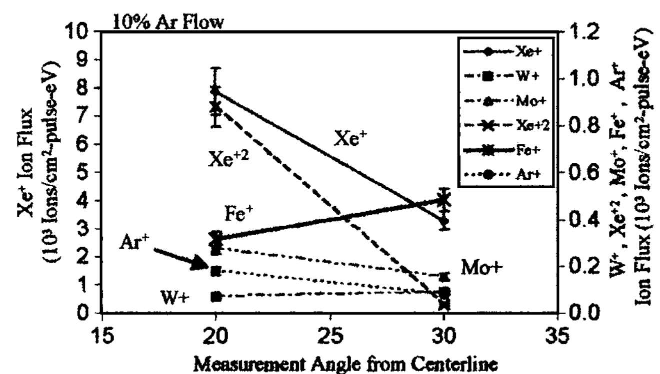

FIG. 24. Angular dependence of ion species measured from the z-pinch centerline, taken at 10% maximum argon flow rate. Ion energy is 4 keV.

Downloaded 30 Nov 2007 to 130.126.32.13. Redistribution subject to AIP license or copyright; see http://jap.aip.org/jap/copyright.jsp

Integrated photodiode measurements indicate a 25% drop in 13.5 nm light intensity from the source at 75% maximum argon gas flow.[14] At 100% flow, the measured decrease is 40%.[14] Possible mechanisms for this decrease in EUV light output may include increased absorption from argon and possibly xenon. The source constantly flows xenon while pulsing at 64 Hz for these experiments. This results in an ambient pressure of ~3 mtorr. Photodiode measurements are made at a distance of 95 cm from the pinch through this background pressure. The ambient pressure is a side effect of the pumping capacity of the chamber. This may not reflect real conditions measured at the mirror location which would be immediately adjacent to the exit of the debris mitigation tool (~25 cm). High-volume manufacturing tools will likely see an increase in the pumping capacity of the source chamber to lower ambient pressure and will operate around 5000 Hz as opposed to 64 Hz, both of which could reduce the absorptive effects described above.

V. CONCLUSIONS

Experiments with a spherical sector energy analyzer on the XTS 13-35 xenon *z*-pinch EUV source have allowed characterization of the direct fast ion debris field. Ions have been characterized with energies up to 15 keV. Typical EUV emission from the *z* pinch is measured and exposure testing of optical samples has been performed up to 1×10^7 pulses.

Species dominating the fast ion debris are Xe^+ and Xe^{+2} which maximize at 8 and 4 keV, respectively. These correspond to the fuel used for the *z* pinch. Other ion species measured include Ar^+, Ni^+, Fe^+, Mo^+, W^+, and Si^+, and are released from sources in the chamber. Trends measured indicate possible optimization of the pinch structure exhibited by increases in xenon ion flux as debris tool argon flow rates are increased. At high argon flow rates (>50% maximum buffer gas flow rate) measured direct ion species drop to unmeasurable levels for the particular setup and sensitivities used. Mirror exposure microanalysis combined with ion debris energy spectra suggests that particle momentum is still being transferred to mirror surfaces despite decreases in measured ion flux with increased argon flow rate. These effects are mitigated extensively through the debris tool as indicated by reflectivity measurements with the debris tool operating.[15] However, more testing is needed to verify this effect.

Future work includes modification of microchannel plate detectors used in the ESA to provide a direct line of sight to the source. A high-voltage deflector system is being constructed to redirect ion motion away from the detectors such that impingement by fast neutral atoms can be measured as a function of time. This will allow assessment of the ultimate operability of debris mitigation techniques since it is currently unknown if measured drops in ion production will translate to a drop in total particle momentum transferred to optical surfaces in the chamber.

ACKNOWLEDGMENTS

This research was partially funded by Intel Components Research, No. SRA03-159, Dr. Robert Bristol, program manager. Partial funding also came from International SEMATECH, Dr. Ginger Edwards, program manager. This research was partially carried out in the Center for Microanalysis of Materials, University of Illinois, which is partially supported by the U.S. Department of Energy under Grant No. DEFG02-91-ER45439. The authors acknowledge XTREME Technologies GmbH and Dr. Tran Duc Chin for their expertise with operation of the plasma source used. We would also like to thank the machine shop at the Department of Theoretical and Applied Mechanics and the machine shop at the Department of Electrical and Computer Engineering at the University of Illinois Urbana-Champaign. Finally we would like to thank Comstock Inc. for conversations regarding operation of the energy sector analyzer.

[1] U. Stamm *et al.*, Proc. SPIE 5374-14 (2004).
[2] M. Richardson, C.-S. Koay, K. Takenoshita, C. Keyser, S. George, S. Teerawattansook, M. Al-Rabban, and H. Scott, Proc. SPIE 5374-112 (2004).
[3] XTREME Technologies GmbH, Gottingen, Germany, www.xtremetec.de
[4] L. A. Shmaenok, C. C. de Bruijn, H. Fledderus, R. Stuik, A. A. Schmidt, D. M. Simanovskii, A. A. Sorokin, T. A. Andreeva, and F. Bijkerk, Proc. SPIE 3331-87 (1998).
[5] C. P. Browne, D. S. Craig, and R. M. Williamson, Rev. Sci. Instrum. **22**, 12 (1951).
[6] J. A. Simpson, Rev. Sci. Instrum. **32**, 12 (1961).
[7] F. R. Paolini and G. C. Theodridis, Rev. Sci. Instrum. **38**, 5 (1967).
[8] Comstock Inc., Oak Ridge, Tennessee, www.comstockinc.com
[9] D. Rogers and R. F. Malina, Rev. Sci. Instrum. **53**, 9 (1982).
[10] Burle Electro-Optics, Sturbridge, Massachusetts, www.burle.com
[11] SPECS Scientific Instruments, Inc., Sarasota, Florida, www.specs.com
[12] D. A. Alman *et al.*, Proc. SPIE 5751-137 (2005).
[13] H. Qiu, D. A. Alman, K. C. Thompson, J. B. Spencer, E. L. Antonsen, B. E. Jurczyk, D. N. Ruzic, and T. P. Spila, J. Microlithogr., Microfabr., Microsyst. (submitted).
[14] K. C. Thompson, E. L. Antonsen, M. R. Hendricks, B. E. Jurczyk, M. Williams, and D. N. Ruzic, Microelectron. Eng. **83**, 3 (2006).
[15] U. Stamm *et al.*, Proc. SPIE 5037-16 (2003).

Downloaded 30 Nov 2007 to 130.126.32.13. Redistribution subject to AIP license or copyright; see http://jap.aip.org/jap/copyright.jsp